Int J Earth Sciences (Geol Rundsch) (2001) 90:118–126
DOI 10.1007/s005310000162

ORIGINAL PAPER

Florian Heidelbach · Iona C. Stretton · Karsten Kunze

Texture development of polycrystalline anhydrite experimentally deformed in torsion

Received: 30 July 2000 / Accepted: 9 October 2000 / Published online: 9 March 2001

Abstract A polycrystalline aggregate of anhydrite was deformed in torsion to a maximum shear strain of 8.1 at 700 °C and a maximum shear strain rate of 5×10^{-3} s^{-1}. The crystallographic preferred orientation (CPO or texture) was investigated as a function of shear strain/shear strain rate in a radial profile from the centre to the edge of the sample. A deformation texture developed at shear strains of 1.5–2 (corresponding to shear strain rates of 1 to 1.3×10^{-3} s^{-1}) and reached a stable position relative to the kinematic frame at a shear strain of 3.7 (2.3×10^{-3} s^{-1}). Further shear strain only led to a small increase in texture strength but no change in the orientation relative to the kinematic frame. The CPO is very similar to naturally observed textures and can be explained by the activity of the {001}<010> and {012}<121> slip systems. Although independent mechanical data indicate that a change of mechanism from dislocation- to diffusion-controlled creep occurred at a shear strain of approximately 1.5, the texture does not weaken, but rather increases, in strength with higher shear strains.

Keywords Anhydrite · Deformation · Torsion · Texture · Slip system

Introduction

Anhydrite ($CaSO_4$) is an important mineral in sedimentary sequences of the upper crust. During deformation, anhydrite-rich layers frequently form the weakest member of the sequence and accommodate the highest strains (e.g. Jordan and Nüesch 1989; Marcoux et al. 1987; Müller and Briegel 1980). The development of crystallographic preferred orientation (CPO or texture) of anhydrite is therefore of interest for the interpretation of the deformation fabrics in these rocks. The following intracrystalline deformation mechanisms have been recognized that may contribute to the development of a CPO in polycrystalline anhydrite (Mügge 1889; Ramez 1976b):

1. Translation glide on {001}<010>;
2. Translation glide on {012}<121>; for this system the positive sense of slip (towards <001>) would be more favourable, e.g. for (012) the $[1\bar{2}1]$ direction;
3. Twinning on the {101} planes; due to the relatively small shear involved (12.5°), twinning cannot accommodate large strains but causes a relatively large reorientation of the crystal lattice (a rotation of 83.5° approximately [001]; Klassen-Neklyudova 1964). Under experimental conditions twinning appears to be of significance only at temperatures between 300 and 600 °C (Dell'Angelo and Olgaard 1995).

Studies of the texture in naturally deformed anhydrite rocks have yielded in most cases a uniform type of CPO, showing a preferential alignment of the {001} planes subparallel to the foliation and <010> parallel to the lineation (Schwerdtner 1970; Mainprice et al. 1993). In shear deformation environments an alignment of {001} and <010> was found with the shear plane and shear direction, respectively (Jordan et al. 1990; Jordan 1992). This CPO is consistent with dominant slip on the {001}<010> slip system. The texture analysis of an evaporite diapir consisting of coarse-grained anhydrite by Mainprice et al. (1993) yielded a CPO which was also consistent with slip on {012}<121>.

The texture development of anhydrite during deformation in axial compression has been investigated in numerous experimental studies (Dell'Angelo and Olgaard 1995; Müller and Siemes 1974; Müller et al. 1981; Ramez 1976a) and correlated with different

F. Heidelbach (✉) · I. C. Stretton
Bayerisches Geoinstitut, Universität Bayreuth,
95440 Bayreuth, Germany
E-mail: florian.heidelbach@uni-bayreuth.de
Phone: +49-921-553730
Fax: +49-921-553769

K. Kunze
Geologisches Institut, ETH Zürich, 8092 Zürich, Switzerland

deformation mechanisms. For deformations at low temperatures, an alignment of the compression axis with the <100> axis was generally observed, which was interpreted to be due mainly to twinning on the {101} planes. Increasing temperature suppressed twinning and by enhancing intracrystalline glide on the slip systems caused a preferred orientation of the <001> directions parallel to the compression axis. At low stresses, slow strain rates and small grain sizes, diffusion creep accompanied by grain-boundary sliding became the dominant mechanism (Dell'Angelo and Olgaard 1995) and no texture developed. Lattice preferred orientations of anhydrite were also examined in deformation experiments with two-phase mixtures (anhydrite–halite by Ross et al. 1987, and anhydrite–calcite by Bruhn and Casey 1997). In both cases the CPOs of anhydrite did not deviate significantly (in strength or pattern) from the textures in single-phase experiments in axial compression.

In the present study we deformed a polycrystalline aggregate of anhydrite in simple shear to high shear strains using the torsion testing technique (Paterson and Olgaard 2000). A sample deformed in torsion exhibits a gradient of strain from the centre of rotation (theoretically zero shear strain) to the outer edge of the sample (maximum strain and strain rate). Therefore, it is possible to follow the texture development as a function of these two parameters within one sample. Due to the intrinsic heterogeneity in a torsion sample, it is, however, necessary to probe the texture with a high-resolution technique. This was achieved here by employing a small synchrotron X-ray beam (30-μm diameter) to perform diffraction experiments in transmission geometry.

Experimental methods

Sample

A polycrystalline aggregate of anhydrite was deformed at 700 °C and a confining pressure of 300 MPa in torsion to a shear strain of 8.1 at a shear strain rate of 5×10^{-3} s^{-1} (both measured at the outer edge of the sample). The development of the maximum stress in the course of the torsion test is displayed in the stress–strain curve for this sample (Fig. 1; Stretton and Olgaard 1997). It shows a peak strength at a shear strain of 1, followed by a softening of the material up to shear strain of 3 and a constant flow stress up to a shear strain of 8. The strain softening was shown to be accompanied by grain-size reduction and independent strain-rate stepping tests demonstrated a change in dominant deformation mechanism from dislocation (stress exponent of $\geq$3) to diffusion (stress exponent of 1) controlled creep (Stretton and Olgaard 1997). This reduction in grain size can be seen in a section cut radially through a sample used in the strain-rate stepping tests (Fig. 2). At the outer edge of the sam-

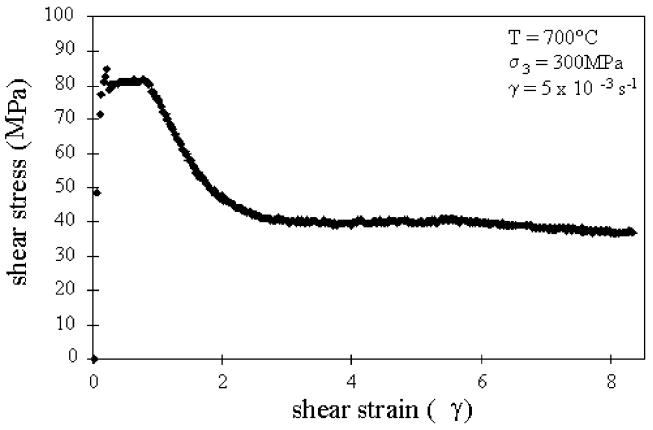

Fig. 1 Stress–strain curve for the investigated sample. The stress refers to the maximum stress at the outer edge of the sample

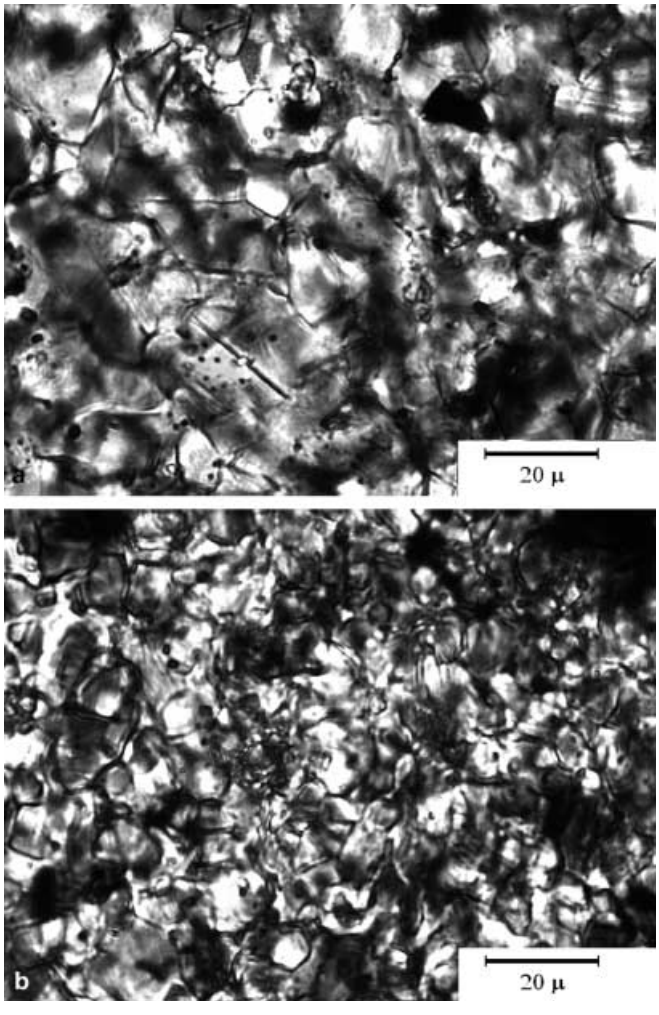

Fig. 2 Optical micrographs of the sample at low strain (**a**, γ~1) and high strain (**b**, γ~7). Note the reduction in grain size with increasing strain; radial section perpendicular to shear plane (*horizontal*) and the shear direction; crossed polarizers

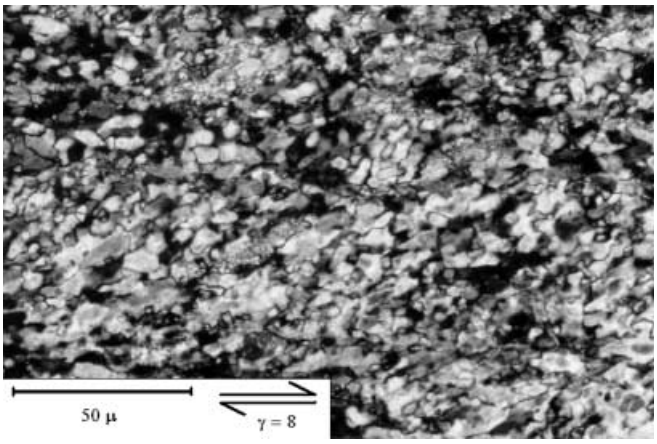

Fig. 3 Optical micrograph of the investigated sample; section is perpendicular to the radial direction, shear plane is horizontal, and shear sense is indicated. Note the grain elongation oblique to the shear plane at an angle of approximately 25°; crossed polarizers

ple used for texture analysis, the most highly strained part, the grain fabric in the tangential section shows an elongation oblique to the shear plane (Fig. 3). The mean grain elongation is approximately 20–30° rotated against the shear sense from the shear direction.

Texture analysis

The texture analysis was carried out at the Microfocus beamline of the European Synchrotron Radiation Facility (Riekel et al. 1992). For the measurement we employed a monochromatic (λ=0.782 Å) synchrotron X-ray beam in combination with a two-dimensional CCD detector. The sample was prepared as a polished slab of approximately 100-µm thickness and measured in transmission geometry. With the two-dimensional detector the intensity variations along Debye-Scherrer diffraction rings, i.e. the deviations from the ideal powder, were utilized to determine the CPO. The synchrotron X-ray beam was focused down to a size of 30 µm, giving sufficient spatial resolution at high intensity. With the two-dimensional CCD detector numerous different diffraction rings could be recorded simultaneously (Fig. 4). Each diffraction ring is generated by lattice planes lying on a small circle with opening angle 90- around the incoming beam. By rotating the sample around a single axis, a partial pole

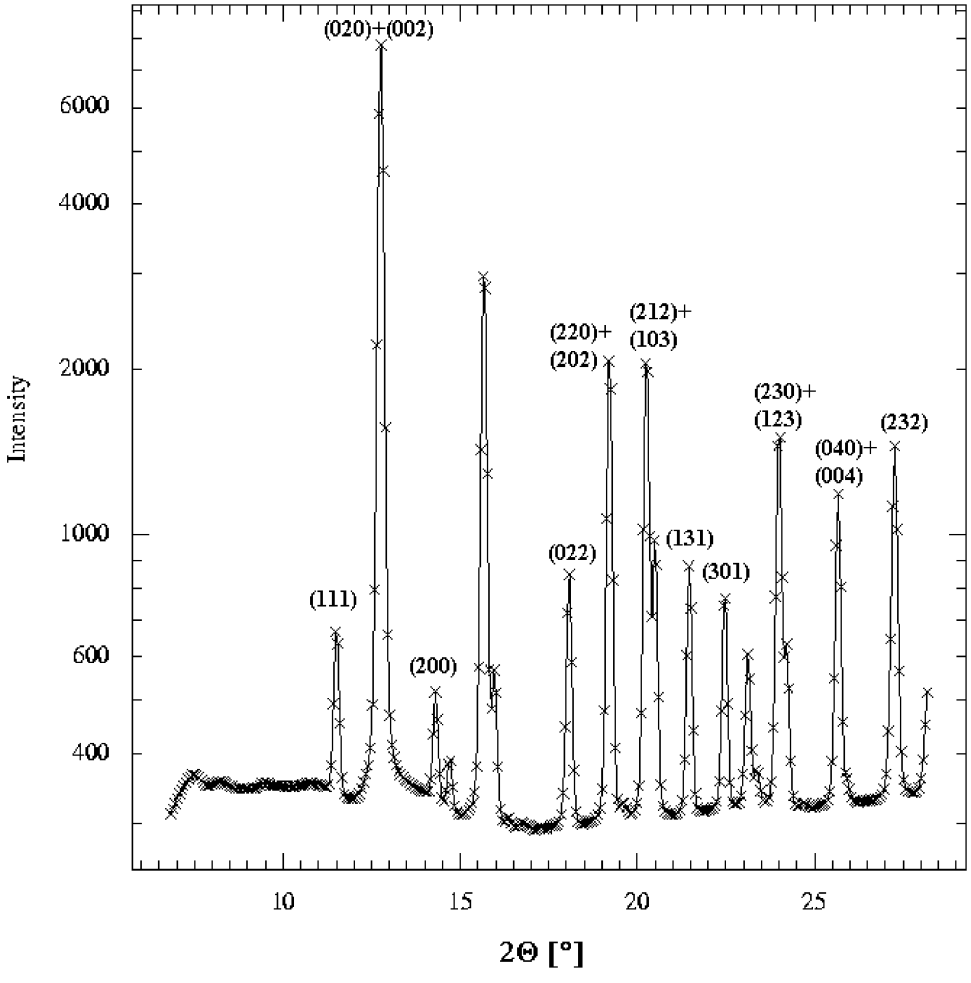

Fig. 4 2 profile extracted from two-dimensional diffraction pattern (λ=0.782 Å). Reflections used for the texture analysis are indicated

figure can be constructed. The sample was rotated perpendicular to the beam up to ±62.5° leading to a lateral width of the measured volume of approximately 200 μm. The measured volume was therefore 30×200×100 μm. In the experimental setup the direction with diminished spatial resolution (200 μm) was aligned perpendicular to the strain gradient (i.e. the radius of the sample).

The details of this texture analysis method are described in Heidelbach et al. (1999). Herein we present just one example on how the analysis was carried out at each measurement point. Partial pole figures of the following 16 lattice planes were derived from the diffraction experiment (Fig. 5): {111}; {020}+{002}; {200}; {022}; {220}+{202}; {212}+{103}; {131}; {301}; {230}+{123}; {040}+{004} and {232}. All 11 pole figures (5 of them overlapped) were used in the calculation of the orientation distribution function (ODF), which gives the complete texture information of the measured volume. The calculation of the ODF was carried out with the iterative WIMV algorithm as it is implemented in the texture package BEARTEX (Wenk et al. 1998). The ODF was then smoothed with a Gaussian function of 10° FWHM (full width half maximum) in order to even out effects from the varying grain size in the different areas of the sample. From the ODF complete pole figures were recalculated and overlapped pole figures could be separated according to the structure factors of the different lattice planes. The crystallographic setting for the orthorhombic anhydrite was chosen such that |a|=6.23 Å, |b|=6.991 Å and ¸|=6.996 Å . This deviates from the setting often found in the mineralogy literature, but it is the convention used in all previous papers about textures in anhydrite, so we chose it to facilitate the comparison with other articles. The lattice parameters b and c of anhydrite are extremely close (6.991 and 6.999Å); therefore, all measured lattice reflections {hkl} with k≠l were a combination of {hkl} and {hlk}. In most cases, however, the structure factor of one of the two lattice planes is much stronger than that of its counterpart. A separation of the pole figures was therefore carried out only if both {hkl} and {hlk} had comparable intensities (within a factor of 20). The recalculated pole figures (Fig. 6) are all consistent with each other and reproduce the main features of the experimental pole figures. In Fig. 7 the contributions to the overlapped pole figures are shown separated; particularly it should be noted that the pole figures of {020} and {002} exhibit clearly distinct orientation patterns.

The crystallographic preferred orientation was measured at distances of 0.4, 0.9, 1.4, 1.9, 2.4, 3.4, 4.4, 5.4, 6.4 and 7.4 mm from the centre of the deformed cylinder, corresponding to shear strains of 0.44, 0.99, 1.54, 2.09, 2.64, 3.74, 4.84, 5.94, 7.04 and 8.14. The texture of a hot-pressed sample (i.e. the starting material) was also measured for comparison. In the figures below it is displayed under γ =0.

Results

The results of the texture analysis are displayed in Figs. 8, 9, 10 and 11, which show the preferred alignment of {002}, {020}, {012} and <121> as a function of increasing shear strain. The hot-pressed sample (γ=0) exhibits no discernible texture. In the deformed sample, measurements close to the centre also do not reveal any clear preferred orientation. A texture pat-

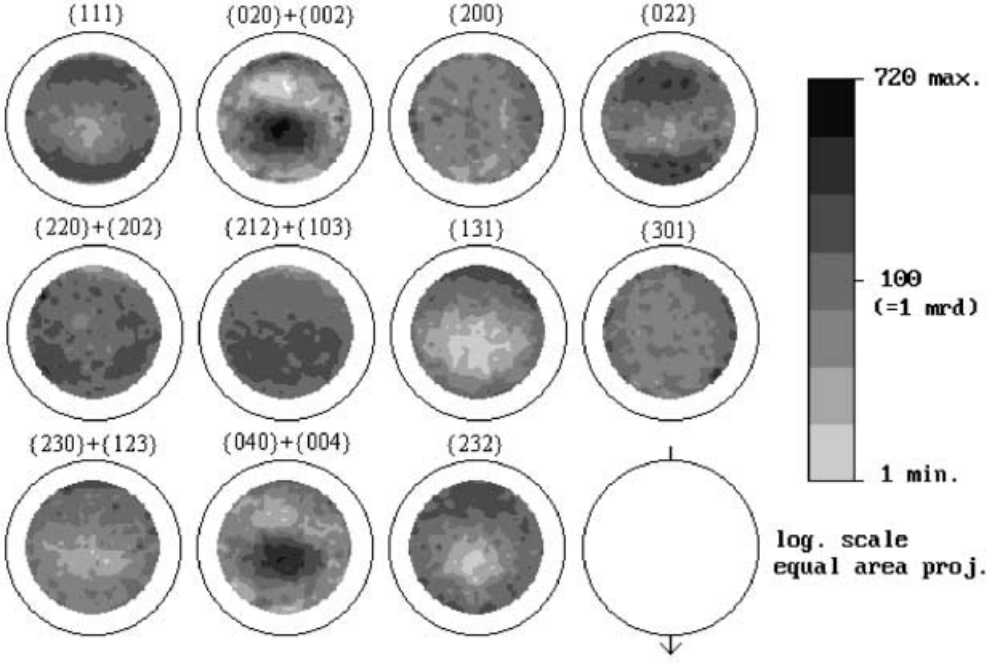

Fig. 5 Incomplete experimental pole figures. The projection (equal area, lower hemisphere) is onto the shear plane, the shear direction is oriented N–S, shear sense is top to the south; *mrd* = multiples of random distribution

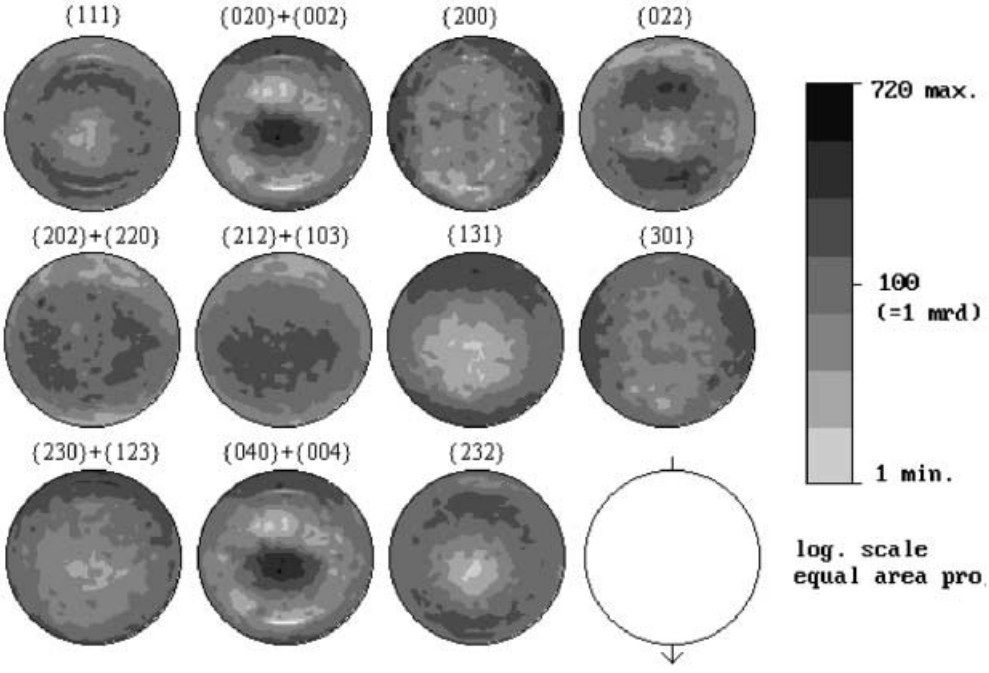

Fig. 6 Complete pole figures, recalculated from the orientation distribution function. The projection (equal area, lower hemisphere) is onto the shear plane, the shear direction is oriented N–S, shear sense is top to the south

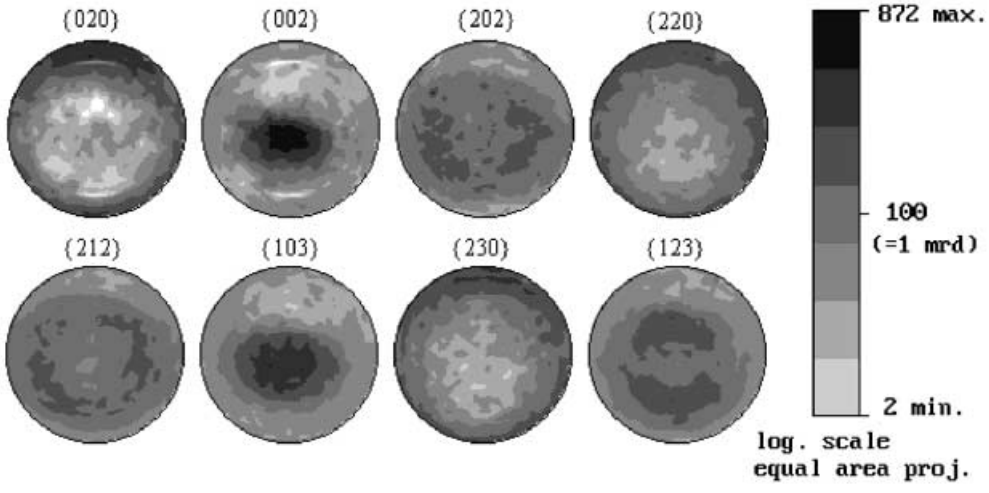

Fig. 7 Separated recalculated pole figures (compare with Fig. 5). Orientation and projection are the same as in Fig. 5

tern arises at shear strains of 1.5–2 (corresponding to strain rates of 1 and 1.3×10^{-3} s^{-1}, respectively). It reaches a stable position relative to the kinematic frame at a shear strain of 3.74 (strain rate 2.3×10^{-3} s^{-1}). The texture is marked by a maximum of normals of the {002} planes at 10–15° to the normal of the shear plane rotated against the shear sense (Fig. 8). The normals of the {020} planes (Fig. 9) form a girdle which lies at an angle of 10–15° relative to the shear plane rotated against the shear sense. The girdle has a maximum close to the shear direction. The normals to the {012} planes (Fig. 10) display a double maximum, one of which is almost parallel to the shear plane normal, whereas the other is rotated approximately 40° away from it against the sense of shear. Similarly, the <121> directions form a double maximum on both sides of the shear direction (Fig. 11). In the outer part of the sample, where the accommodated shear strains and shear strain rates are the highest, the CPO displays only a slight sharpening and a small increase in strength of the same texture.

Discussion

For both slip systems the glide planes ({001} and {012}; Figs. 8, 10) are in a position close to the macroscopic shear plane of the experimental setup, i.e. in an orientation with high resolved shear stress. Also the glide directions of the two slip systems (<010> and <121>; Figs. 9, 11) show an approximate alignment with the macroscopic shear direction. Both slip systems are therefore aligned close to the so-called easy slip position, which maximizes the resolved shear stress on the

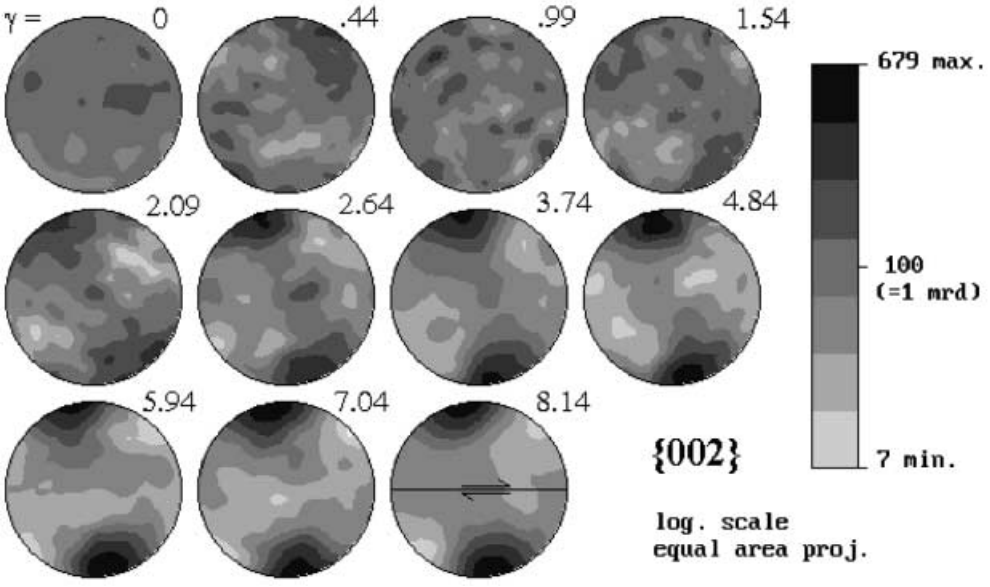

Fig. 8 Pole figures of {002} as a function of shear strain. The shear plane is horizontal and perpendicular to the surface of the page, the dextral shear sense is indicated; lower hemisphere, equal area projection

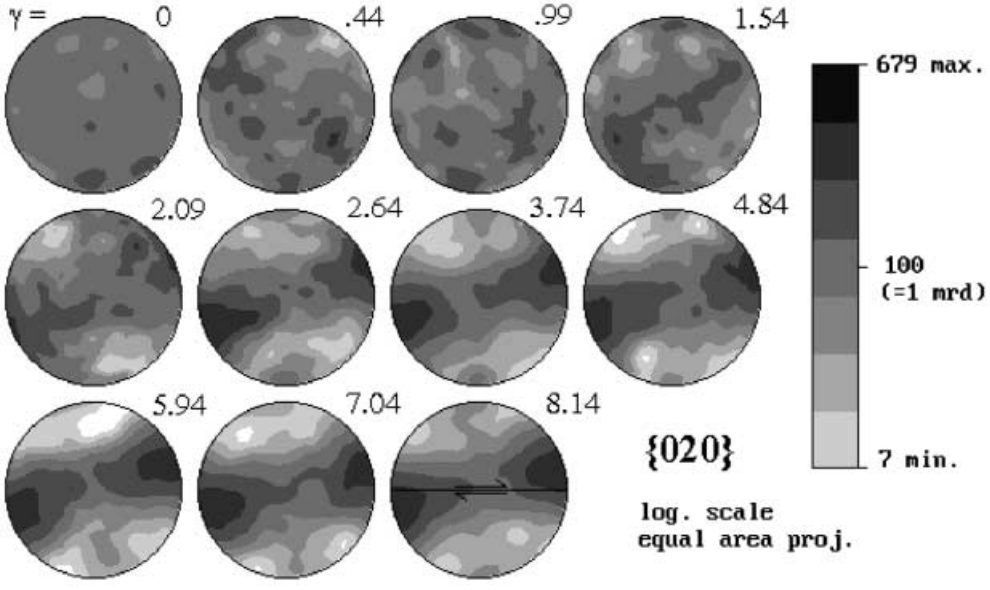

Fig. 9 Pole figures of {020} as a function of shear strain. The shear plane is horizontal and perpendicular to the surface of the page, the dextral shear sense is indicated; lower hemisphere, equal area projection

slip system, indicating that both intracrystalline slip systems were active during deformation. Both slip systems start to show significant alignment in the described orientations at a shear strain of approximately 2 (Figs. 8, 9, 10, 11). The higher intensities for the {002} and {020} pole figures in comparison the the pole figures of {012} and <121> are simply due to the higher multiplicity of the latter in the orthorhombic crystal structure and are therefore not indicative of a stronger alignment of one slip system relative to the other. Due to the lack of simulation of texture development in this material with models of polycrystal plasticity (e.g. Kocks et al. 1998), a more quantitative approach to an interpretation of this texture is not possible presently.

Comparison with naturally occurring anhydrite textures

The observed texture pattern corresponds well with preferred lattice orientations encountered in natural anhydrite mylonites. It is clearly oblique to the kinematic reference frame (approximately 10–15° *against* the sense of shear). Relative to the long axes of the ellipsoidal grains (Fig. 3), however, the texture pattern appears to be rotated approximately 10–15° *with* the sense of shear. A similar obliqueness of the texture is observed in the studies by Jordan et al. (1990) and Mainprice et al. (1993) indicating that their reference frame for the texture analysis may have been related to the grain fabric and not to the kinematic framework. A clear difference to the CPOs shown by Mainprice et al. (1993) lies in the {002} and {020} pole fig-

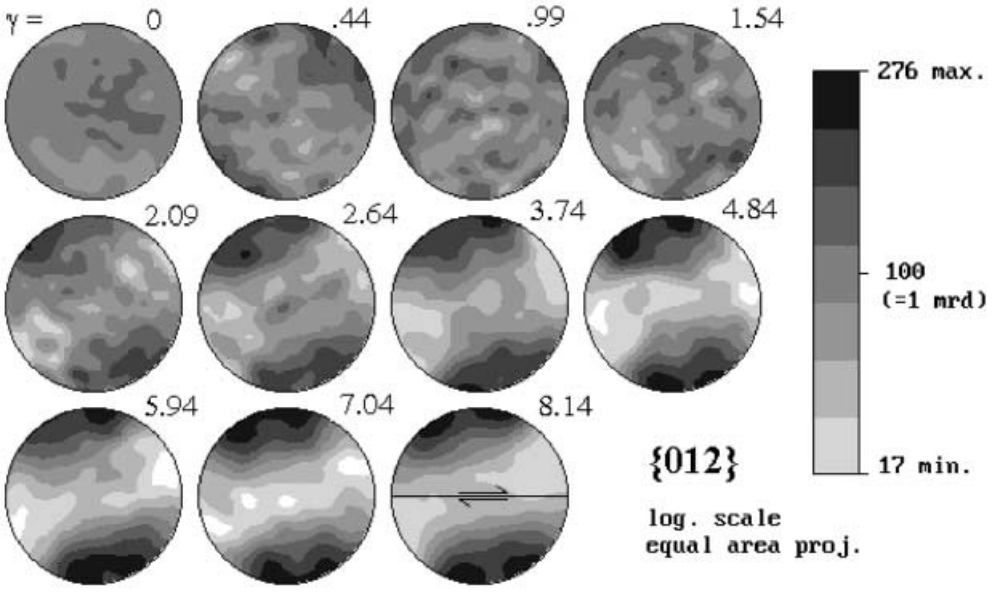

Fig. 10 Pole figures of {012} as a function of shear strain. The shear plane is horizontal and perpendicular to the surface of the page, the dextral shear sense is indicated; lower hemisphere, equal area projection

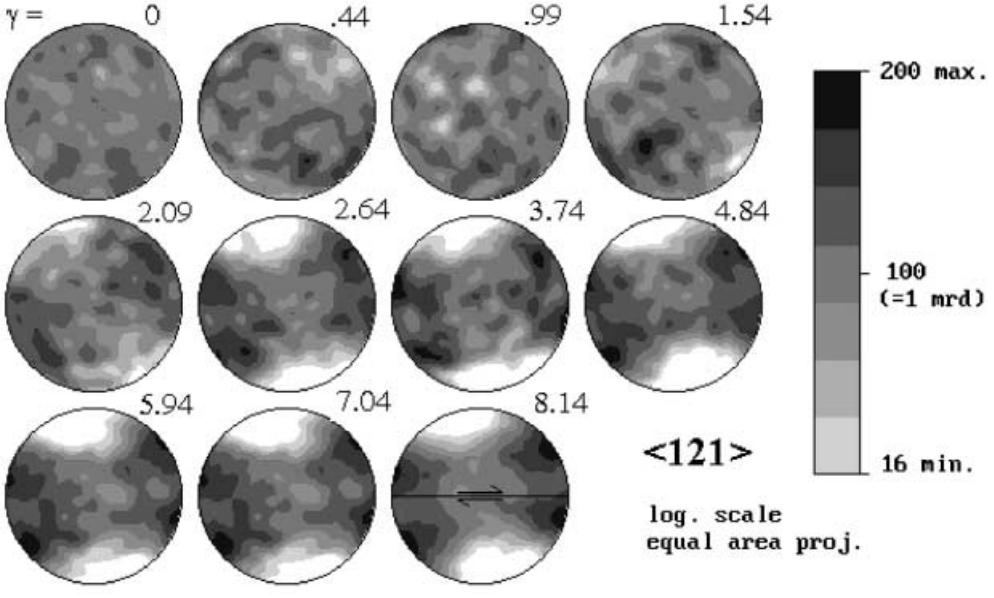

Fig. 11 Stereographic projection of <121> as a function of shear strain. The shear plane is horizontal and perpendicular to the surface of the page, the dextral shear sense is indicated; lower hemisphere, equal area projection

ures. In their study the girdle fabric is displayed by the {002} pole figure and the {020} pole figure shows a single maximum, which is the opposite of the CPO in our case (compare with Figs. 8 and 9). Similar effects are visible for the {012}<121> slip system. The slip planes form two isolated maxima, whereas the maxima of the shear directions are connected by two weak girdles. The reason for this is not clear. A possible explanation would be that some intracrystalline glide occurred on the {001} planes in a direction different from <010>.

Correlation with the experimental stress–strain curve

The shape of the stress–strain curve in Fig. 1 describes the mechanical behaviour of the outermost radius of the sample. The shear strain and hence shear strain rate decrease linearly towards the axis of the sample cylinder. The variation of the shear strain rate spans approximately one order of magnitude from 2.7×10^{-4} s^{-1} at γ=0.44 (close to the centre of the cylinder) to 5×10^{-3} s^{-1} at γ =8.14 (outer radius of the sample). For this range of strain rates, the influence of strain rate on the deformation behaviour is small and does not induce a change in deformation mechanism (Dell'Angelo and Olgaard 1995). When a change in defor-

mation mechanism occurs during a single experiment, e.g. brought about by grain-size reduction through dynamic recrystallization (Fig. 2), it is possible that the outer and centre volumes may deform by different mechanisms. Therefore, the assumption appears reasonable that the textures in different parts of the sample can be correlated with different stages in the stress–strain curve and different deformation mechanisms.

The first stage of deformation, in which dislocation creep is the dominant deformation mechanism (up to a shear strain of 1), seems to have produced relatively little CPO in the sample. This slow development of a significant CPO is possibly due to the small radius of the sample in this area, which causes a more heterogeneous microstructure and texture. In our sample a significant texture appears to have formed at shear strains of approximately 1.5–2.6, i.e. during the transition phase where significant softening occurs and a grain-size reduction (from 12 to 6 μm) by dynamic recrystallization took place. The grain-size reduction led to a change in the dominant deformation mechanism from dislocation to diffusion-controlled creep. At higher shear strains (>2.6) the grain size and the texture remain constant indicating that texture and microstructure have reached a steady state. It appears that diffusion-controlled creep, which is the dominant mechanism in this phase of the deformation, does not lead to a weakening of the texture.

Similar observations were made by Rutter et al. (1994) in axial compression and extension experiments with calcite marbles. They found that a preexisiting CPO in this material was preserved despite a subsequent deformation in the grain-size sensitive superplastic flow regime. In simple shear experiments with the analogue material norcamphor, Herwegh et al. (1997) found a steady-state texture and microstructure forming at high shear strains (γ>8). They related this texture to predominant grain-boundary migration recrystallization; however, from their experimental setup mechanical data could not be extracted so that it is not clear if the samples reached the diffusional creep regime.

Our results appear to be in contradiction to the general assumption that materials deformed in diffusion-controlled creep do not develop a significant CPO (e.g. Karato and Wu 1993). A possible explanation is that our sample already had a texture when it started to deform in diffusion-controlled creep (similar to the experiments of Rutter et al. 1994). There is no obvious reason why diffusion-controlled creep should obliterate a pre-existing texture in the sample, particularly since the orientation of the external stresses remained unchanged during the deformation experiment. The results presented here indicate that a CPO may be preserved or even strengthened during relatively long periods of diffusion-controlled creep.

Conclusion

The experimentally sheared sample of anhydrite exhibits a crystallographic preferred orientation that is very close to textures observed in naturally deformed anhydrite. The correlation of the texture development with increasing strain indicates that the formation of the deformation texture starts at shear strains of approximately 1.5–2.6. In the stress–strain curve this is the region where significant softening of the sample is observed after which a change in deformation mechanism from dislocation to diffusion diffusion-controlled creep controlled creep occurs. The position of the texture relative to the kinematic frame remains constant up to the maximum shear strain achieved in the sample. Although diffusion-controlled creep is the dominant deformation mechanism at higher strains, the crystallographic preferred orientation was not weakened but rather increased in strength.

Acknowledgements We acknowledge the constructive reviews of J. Urai and an anonymous reviewer. Deformation of the sample was carried out at ETH Zürich under the grant number NF 2100-045646.95.

References

Bruhn DF, Casey M (1997) Texture development in experimentally deformed two-phase aggregates of calcite and anhydrite. J Struct Geol 19:909–925

Dell'Angelo LN, Olgaard DL (1995) Experimental deformation of fine-grained anhydrite: evidence for dislocation and diffusion creep. J Geophys Res 100B:15425–15440

Heidelbach F, Riekel C, Wenk HR (1999) Quantitative texture analysis of small domains with synchrotron X-rays. J Appl Crystallogr 32:841–849

Herwegh M, Handy MR, Heilbronner R (1997) Temperature- and strain-rate-dependent microfabric evolution in monomineralic mylonite: evidence from in situ deformation of norcamphor. Tectonophysics 280:83–106

Jordan P (1992) Evidence for large-scale decoupling in the Triassic evaporites of northern Switzerland: an overview. Eclog Geol Helv 85:677–693

Jordan P, Nüesch R (1989) Deformation structures in the Muschelkalk anhydrites of the Schafisheim Well (Jura overthrust, northern Switzerland). Eclog Geol Helv 82:429–454

Jordan P, Noack T, Widmer T (1990) The evaporite shear zone of the Jura Boundary Thrust–new evidence from Wisen well (Switzerland). Eclog Geol Helv 83:525–542

Karato SI, Wu P (1993) Rheology of the Upper Mantle: a synthesis. Science 260:771–778

Klassen-Neklyudova MV (1964) Mechanical twinning of crystals. Consultants Bureau, New York, pp 1–87

Kocks UF, Tomé CN, Wenk H-R (1998) Texture and anisotropy. Cambridge University Press, Cambridge, pp 1–676

Mainprice D, Bouchez JL, Casey M, Dervin P (1993) Quantitative texture analysis of naturally deformed anhydrite by neutron diffraction texture goniometry. J Struct Geol 15:793–804

Marcoux J, Brun JP, Burg JP, Ricou LE (1987) Shear structures in anhydrite at the base of thrust sheets (Antalya, southern Turkey). J Struct Geol 9:555–561

Mügge O (1889) Über Translationen und verwandte Erscheinungen in Krystallen. Neues Jahrbuch der Mineralogie, Geol Paläontol 1:71–162

Müller P, Siemes H (1974) Festigkeit, Verformbarkeit, und Gefügeregelung von Anhydrit – Experimentelle Stauchverformung unter Manteldrucken bis 5kbar bei Temperaturen bis 300 °C. Tectonophysics 23:105–127

Müller WH, Briegel U (1980) Mechanical aspects of the Jura overthrust. Eclog Geol Helv 73:239–250

Müller WH, Schmid SM, Briegel U (1981) Deformation experiments on anhydrite rocks of different grain sizes: rheology and microfabric. Tectonophysics 78:527–543

Paterson MS, Olgaard DL (2000) Rock deformation tests to large shear strains in torsion. J Struct Geol 22:1341–1358

Ramez MRH (1976a) Fabric changes in experimentally deformed anhydrite rocks. N Jahrb Mineral Abh 128:89–113

Ramez MRH (1976b) Mechanisms of intragranular gliding in experimentally deformed anhydrite. N Jahrb Mineral Abh 127:311–329

Riekel C, Bösecke P, Sanchez del Rio M (1992) Two high brilliance beam lines at the ESRF dedicated to microdiffraction, biological crystallography, and small-angle scattering. Rev Sci Inst 63:974–981

Ross JV, Bauer SJ, Hansen FD (1987) Textural evolution of synthetic anhydrite–halite mylonites. Tectonophysics 140:307–326

Rutter EH, Casey M, Burlini L (1994) Preferred crystallographic orientation development during the plastic and superplastic flow of calcite rocks. J Struct Geol 16:1431–1446

Schwerdtner WM (1970) Gitterorientierungs-Mechanismus in Anhydrit-Schiefer. In: Paulitsch P (ed) Rock deformation. Springer, Berlin Heidelberg New York, pp 142–164

Stretton IC, Olgaard DL (1997) A transition in deformation mechanism through dynamic recrystallization: evidence from high strain, high temperature torsion. AGU Fall Meeting. Eos Trans:F723

Wenk HR, Matthies S, Donovan J, Chateigner D (1998) BEARTEX: a Windows-based program system for quantitative texture analysis. J Appl Crystallogr 31:262–269